*Acta Pharm.* **76**(3) (2026) 260013 (xx pages)

https://doi.org/10.2478/acph-2026-0013

Article

# Freeze-dried kit formulation and physicochemical assessment of a daratumumab-based radiopharmaceutical

PAULINA APOSTOLOVA[1]
MARIJA ATANASOVA LAZAREVA[1,2]
KATARINA DAVALIEVA[3]
MARIJA AREV[1]
DINO KARPICAROV[1]
PETRE MAKRESKI[4]
IRENA SLAVESKA SPIREVSKA[5]
IVANA MITREVSKA[1,7]
ALEKSANDAR DIMOVSKI[3]
SANJA VRANJEŠ-ĐURIĆ[6]
EMILIJA JANEVIK-IVANOVSKA[1,*]

[1] *Faculty of Medical Sciences, Goce Delcev University, 2000 Stip, North Macedonia*

[2] *University Institute of Positron Emission Tomography, 1000 Skopje, North Macedonia*

[3] *Research Centre for Genetic Engineering and Biotechnology "Georgi D Efremov", Macedonian Academy of Sciences and Arts, 1000 Skopje, North Macedonia*

[4] *Institute of Chemistry, Faculty of Natural Sciences and Mathematics, Ss. Cyril and Methodius University in Skopje, 1000 Skopje, North Macedonia*

[5] *Replek Farm Ltd., 1000 Skopje, North Macedonia*

[6] *VINČA Institute of Nuclear Sciences, National Institute of the Republic of Serbia, University of Belgrade, 11000 Belgrade, Serbia*

[7] *Quality Assurance, ALKALOID AD Skopje, 1000 Skopje, North Macedonia*

[*]Correspondence; e-mail: emilija.janevik@ugd.edu.mk

Uncorrected proofs

## ABSTRACT

Daratumumab is a fully human anti-CD38 monoclonal antibody with strong potential as a targeting vector for therapeutic radionuclides. This study aimed to develop a freeze-dried daratumumab immunoconjugate kit by selecting a suitable chelator (DOTA-NHS, *p*-SCN-Bn-DOTA, or *p*-SCN-Bn-1B4M-DTPA) for $^{177}$Lu-labeling, optimizing the freeze-drying formulation, and evaluating the physicochemical properties and purity profiles. Conjugation performed in carbonate buffer at elevated temperature enhanced chelator incorporation, and supported selection of daratumumab–*p*-SCN-Bn-DOTA as the most suitable candidate, achieving radiolabeling yield up to 99.8 % without additional purification. Among the evaluated freeze-dried formulations, a saline-based, buffer-free sucrose–mannitol formulation containing polysorbate 20 (S.F5) provided the most favorable characteristics, including minimal residual moisture and the highest monomer purity with non-detectable HMWS species under the applied SE-HPLC conditions. ATR-FTIR and Raman spectroscopy confirmed preservation of the antibody structural integrity after conjugation and freeze-drying. In an *in vitro* study using human serum, [$^{177}$Lu]Lu-daratumumab-*p*-SCN-Bn-DOTA was shown to maintain higher radiochemical purity over 168 h compared to [$^{177}$Lu]Lu-daratumumab-*p*-SCN-Bn-1B4M-DTPA, indicating greater stability. These results support the feasibility of a ready-to-use freeze-dried daratumumab–*p*-SCN-Bn-DOTA kit for $^{177}$Lu-labeling.



*Keywords*: daratumumab, immunoconjugate, $^{177}$Lu-radiopharmaceutical, ready-to-use kit formulation, freeze-drying, physicochemical characterization

Accepted May 4, 2026
Published online May 5, 2026


## INTRODUCTION

Recent advances in cancer therapy have demonstrated the central role of monoclonal antibodies (mAbs), both as stand-alone therapeutics and as a key component of innovative combination strategies (1). Beyond their immunological functions, mAbs can serve as selective carriers for therapeutic radionuclides, an approach known as radioimmunoconjugate (RIC) therapy. This strategy allows targeted delivery of radionuclide-conjugated antibodies to tumor cells, while minimizing radiation exposure to surrounding healthy tissues (2). The clinical value

Uncorrected proofs

of this concept has been previously established and confirmed by $^{90}$Y-ibritumomab tiuxetan and $^{131}$I-tositumomab (3, 4).

Multiple myeloma is a malignant clonal plasma cell disorder characterized by a biologically and clinically heterogeneous spectrum ranging from asymptomatic (smoldering) to symptomatic disease, defined by the presence of myeloma-defining events, including CRAB features and SLiM biomarkers. Despite advances in classification and risk stratification, multiple myeloma remains challenging to treat due to its biological heterogeneity, the development of resistance to standard therapies, and the cumulative toxicity of conventional chemotherapy (5-7).

Daratumumab, a fully human IgG1κ monoclonal antibody (Darzalex, approved for *i.v.* administration by the EMA in 2016; Darzalex Faspro, approved for *s.c.* administration by the FDA in 2020), and isatuximab, a humanized IgG1 monoclonal antibody (Sarclisa, approved for *i.v.* administration by the EMA in 2020), target CD38, a transmembrane ectoenzyme highly expressed on multiple myeloma cells (8-11). Their antitumor activity is mediated through multiple immune-dependent mechanisms, including antibody-dependent cellular cytotoxicity (ADCC), complement-dependent cytotoxicity (CDC), antibody-dependent cellular phagocytosis (ADCP), and direct induction of apoptosis. Both agents exhibit a comparable, generally manageable safety profile characterized by infusion-related reactions, infections, and hematologic toxicities (12-16).

Beyond its use as a native antibody, daratumumab has also been investigated as a vector for targeted radionuclide therapy. Preclinical studies with β$^-$-emitting $^{177}$Lu-DOTA-daratumumab, α-emitting $^{225}$Ac-daratumumab, and $^{212}$Pb-daratumumab have demonstrated enhanced antitumor effects in disseminated multiple myeloma models (17-19). For diagnostic application, conjugates with positron-emitting radionuclides, such as $^{89}$Zr-DFO-daratumumab and $^{64}$Cu-DOTA-daratumumab, have enabled specific immunoPET imaging of CD38-positive malignancies (20, 21). Furthermore, the integration of diagnostic and therapeutic radionuclides within a single vector molecule constitutes the basis of the theranostic approach, a key concept in modern precision medicine, that embodies the principle of "see what you treat and treat what you see" (22). Paired $^{89}$Zr/$^{177}$Lu-daratumumab has demonstrated the potential of a theranostic approach that integrates immunoPET imaging with targeted radioimmunotherapy in preclinical studies (23).

Uncorrected proofs

In this context, a freeze-dried kit formulation offers a practical strategy for standardized preparation of antibody-based immunoconjugates, enabling reproducible radiolabeling at the point of use. Overall, these findings provide a strong rationale for the present study, which aims to develop a daratumumab–based immunoconjugate kit suitable for $^{177}$Lu labeling. These chelators were selected to represent both macrocyclic (DOTA) and acyclic (DTPA-based) systems commonly used for radiometal labeling of antibodies, enabling comparison of radiolabeling efficiency, complex stability, and impact on antibody integrity. The physicochemical properties and structural integrity of the immunoconjugate were evaluated using chromatographic, spectroscopic, and electrophoretic techniques, as well as radiolabeling efficiency.

## EXPERIMENTAL

*Conjugation of daratumumab with BFCs*

The commercially available antibody daratumumab (400 mg/20 mL solution for *i.v.* injection, Janssen Biologics B.V., The Netherlands) was purified by repeated ultrafiltration (30 min, 5000 rpm) on a 30 kDa cut-off filter (Amicon® Ultra, Merck KGaA, Germany). Buffer exchange was performed with 0.1 mol $L^{-1}$ phosphate buffer (pH 8.0). Three commercially available bifunctional chelators (BFCs), *p*-SCN-Bn-DOTA (2-(4-isothiocyanatobenzyl)-1,4,7,10-tetraazacyclododecane-1,4,7,10-tetraacetic acid), DOTA-NHS ester (1,4,7,10-tetraazacyclododecane-1,4,7,10-tetraacetic acid mono-*N*-hydroxysuccinimide ester) and *p*-SCN-Bn-1B4M-DTPA (2-(4-isothiocyanatobenzyl)-6-methyl-diethylene-triamine pentaacetic acid), were evaluated to identify the most suitable chelator for subsequent $^{177}$Lu-labeling.

Conjugation reactions were performed using 20-, 30-, and 50-fold molar excess of each BFC. According to the first protocol, the reaction mixtures were gently shaken and incubated at 4 °C for 16 h (24). In a second protocol, the phosphate buffer was replaced with 0.1 mol $L^{-1}$ carbonate buffer at pH 8.5, and the samples were incubated at 37 °C for 1.5 h (18). After completion of the reaction, the resulting immunoconjugates were purified by repeated ultrafiltration (30 min, 5000 rpm) using 0.15 mol $L^{-1}$ ammonium acetate (pH 7.0) to remove the unbound chelator. The final immunoconjugate concentration was determined spectrophotometrically at 280 nm (UV-1600PC, VWR, USA).

*Freeze-drying formulations (F1-F5)*

Uncorrected proofs

Two batches, each comprising five formulations, were prepared and adjusted to the immunoconjugate concentration of 1 mg $mL^{-1}$. In both batches, formulations F1 and F2 differed only in buffer strength, and both contained 1 % (*m/V*) mannitol as a bulking agent. All remaining formulations were buffer-free. Formulations F3 and F4 contained mannitol and sucrose at different ratios, whereas formulation F5 additionally included polysorbate 20 as a surfactant. Ultra-pure water produced in-house (TKA MicroPure-ST system, Germany) was used as the main solvent for the first batch (Batch W.F1-5). In the second batch (Batch S.F1-5), the identical formulations were prepared using 0.9 % (*m/V*) saline solution (Alkaloid A.D., North Macedonia) as the main solvent. The detailed composition of all formulations, expressed as molar ratios, is provided in Table I.

*Determination of chelator-to-antibody ratio (CAR)*

The average number of chelator molecules conjugated per antibody (chelator-to-antibody ratio, CAR) was determined by matrix-assisted laser desorption/ionization time-of-flight (MALDI–TOF) mass spectrometry using an Axima Performance (Shimadzu, Japan).

The pure freeze-dried antibody and various preparations of bifunctional chelating agents were suspended in 1 mL of ultrapure $H_2O$ and washed 3 times using Amicon® 30 kDa (Merck) to remove salts. The pure samples were reduced to 20 µL, and 80 µL of resuspension solution (30 % ACN/70 % 0.1 mol $L^{-1}$ TFA) was added. An aliquot of 1 µl of the final sample was applied to the sample target and immediately covered by 1 µL of matrix (20 mg $mL^{-1}$ sinapinic acid in 50 % ACN/50 % 0.1 mol $L^{-1}$ TFA). Operational conditions for the MALDI-TOF instrument were set as follows: mode of operation - linear, polarity - positive, max laser rep rate 1, laser power 85, pulsed extraction: 150000, acquisition mass range 100-300000 Da. Peak processing parameters were as follows: peak width 80 chans, chosen to accommodate the relatively broad peak shapes characteristic of linear mode measurements, smoothing method - average, peak detection method - gradient centroid.

*Freeze-drying protocol*

Freeze-drying was performed using a FreeZone 6 liter freeze dryer equipped with a stoppering tray (Labconco, USA). Type I glass vials containing 1 mL of each formulation were partially stoppered with 13-mm butyl rubber stoppers and loaded on precooled shelves at 4 ºC. The shelf-temperature, chamber pressure, hold times for each segment, and a graphical representation are summarized in Table II and Fig. S1.

*Freeze-dried immunoconjugates sample analysis*

Uncorrected proofs

Physicochemical and structural characterization was performed to evaluate the quality of the freeze-dried immunoconjugates and to assess the impact of the formulations and freeze-drying process on the final product.

*Product appearance and reconstitution time*

The freeze-dried formulations were photographed in a black photo box, and their macroscopic appearance was visually assessed. Reconstitution time was determined by dissolving the products in 1 mL of 0.9 % (*m/V*) saline.

*Residual moisture*

Residual moisture, as a key quality attribute of the freeze-dried product, was determined by Karl Fischer volumetric titration using a Compact V20S titrator (Mettler Toledo, USA). Samples of ~20 mg were prepared under controlled-humidity conditions at 25 ºC. Sample handling time was minimized, and vials were opened immediately before analysis to reduce moisture uptake.

*Purity*

The purity and aggregation profile were analyzed by size-exclusion high-performance liquid chromatography (SE-HPLC) using a Waters Alliance e-2695 system coupled with a UV/Vis Waters 2489 detector (Waters Corporation, USA). Isocratic elution was performed on an XBridge Premier Protein SEC column (250 Å, 2.5 µm, 7.8 i.d. x 300 mm) at 25 ºC, for 25 minutes. The mobile phase consisted of 50 mmol $L^{-1}$ phosphate buffer (pH 6.8), 150 mmol $L^{-1}$ NaCl, 50 mmol $L^{-1}$ KCl, with 10 % (*V/V*) ACN, at a flow rate of 0.5 mL $min^{-1}$. A volume of 10 µL of reconstituted sample was injected after filtration through a low protein-binding PVDF membrane filter. Data were processed in Empower 3 software.

*Structure integrity – ATR-FTIR and Raman*

To assess secondary structural changes, Fourier-transform infrared (FTIR) spectra of freeze-dried samples were recorded using a Cary 630 equipped with a diamond attenuated total reflection (ATR) accessory (Agilent Technologies, USA) in the 2000–400 $cm^{-1}$ spectral range. Spectral resolution was set to 4 $cm^{-1}$ with 64 accumulated scans. MicroLabPC software was used for data acquisition and initial spectral processing. The placebo sample was recorded under the same conditions.

In parallel, Raman spectroscopy was used to further verify the higher structural integrity of the immunoconjugates, following a previously published protocol (25).

Uncorrected proofs

*Electrophoresis*

Sodium dodecyl sulfate-polyacrylamide gel electrophoresis (SDS-PAGE) was performed using the MultiGel Long system (Biometra, USA) under reducing and non-reducing conditions. Freeze-dried immunoconjugate and daratumumab (control) were reconstituted in 0.9 % saline and mixed with loading buffer. For reducing conditions, β-mercaptoethanol was added to the samples, and the samples were heated at 95 °C for 5 minutes. Non-reducing samples were incubated at 30 °C without β-mercaptoethanol. A prestained protein ladder (10–180 kDa, Thermo Fisher Scientific, USA) served as the molecular mass standard.

Discontinuous gels were prepared as 4 % stacking gel and either a 12 % (reducing) or a 6 % (non-reducing) resolving gel, using an acrylamide/bis-acrylamide solution (29:1). Proteins were visualized by staining with Coomassie Brilliant Blue R-250 followed by destaining until a clear background was obtained.

*Radiolabeling and* in vitro *stability*

Radiolabeling was performed after reconstitution of the freeze-dried samples in various solvents: a solution of ascorbic acid (0.1 g $mL^{-1}$, *m/V*), 0.1 mol $L^{-1}$ sodium acetate and saline. The pH was adjusted to 4.5, and the immunoconjugates were labeled by adding approximately 11-20 MBq n.c.a. $^{177}LuCl_3$ in aqueous 0.04 mol $L^{-1}$ HCl (EndolucinBeta 40 GBq $mL^{-1}$, ITM, Germany n.c.a), at 37 °C with gentle shaking, for a period of 60 minutes.

The labeling efficiency was estimated by the ratio of total-to-labeled antibody radioactivity with [$^{177}$Lu]Lu-daratumumab-*p*-SCN-Bn-DOTA as a representative sample, by instant thin-layer chromatography (iTLC) using silica gel (SG) strips (Agilent Technologies) and 0.1 mol $L^{-1}$ sodium acetate buffer (pH 4.5) as the mobile phase. Aliquots (10 µL) were spotted, and the chromatograms were scanned with a Scan-RAM radio-TLC scanner (LabLogic Group, UK) and analyzed using Laura 6 software. The same iTLC procedure was used to determine the radiochemical yield of the labeled product.

Subsequently**,** the *in vitro* stability of [$^{177}$Lu]Lu-daratumumab-*p*-SCN-Bn-DOTA and [$^{177}$Lu]Lu-daratumumab-*p*-SCN-Bn-1B4M-DTPA were assessed in human serum at room temperature. Samples were examined every 24 h up to 168 h, and radiochemical purity was determined as previously described.

## RESULTS AND DISCUSSION

Uncorrected proofs

To achieve efficient radiolabeling, the average CAR was first determined as a key predictor of conjugation efficiency (26). Accordingly, the CAR number was quantified by MALDI-TOF and compared across BFCs, molar excesses and conjugation conditions, and was related to the $^{177}$Lu radiolabeling yield of the daratumumab-immunoconjugates. Based on a previously published approach for daratumumab, the initial conjugation was performed using a 10-fold molar excess of DOTA-NHS in phosphate buffer (pH 8.0) (21). However, neither the conjugation reaction nor the subsequent radiolabeling provided satisfactory results. Therefore, additional conjugations were performed using macrocyclic *p*-SCN-Bn-DOTA, DOTA-NHS, and an acyclic *p*-SCN-Bn-1B4M-DTPA, with 20-, 30- and 50-fold molar excesses for each of the three BFCs, and extended to different conditions, using a carbonate buffer (pH 8.5).

The results presented in Table III and Fig. 1 clearly demonstrate that a carbonate buffer and elevated temperature (37 °C) with gentle shaking, compared with a phosphate buffer, improved conjugation, resulting in consistently higher CAR values. Under these conditions, daratumumab-DOTA-NHS showed low CAR overall, with the highest value at a 50-fold excess (reaching CAR value of 0.46 in carbonate buffer pH 8.5), indicating that lower ratios may not give efficient labeling. Considering the published findings that optimal CAR range is commonly within 1-3 (26-28), daratumumab–*p*-SCN-Bn-DOTA conjugates prepared at 20- and 30-fold molar excess were selected for formulation and further experiments. Although daratumumab-*p*-SCN-Bn-1B4M-DTPA showed a similarly low CAR, the 20- and 30-fold excesses were selected for further evaluation, whereas the 50-fold excess was excluded because its CAR was comparable to that of the 30-fold excess. Furthermore, a related immunoconjugate (daratumumab-*p*-SCN-Bn-CHX-DTPA) has been reported using only a 5- to 10-fold excess, supporting that a high excess is not desired (23).

Overall, MALDI-TOF comparison of native daratumumab and its corresponding immunoconjugates showed CAR values ranging from 0 to 3.77, and only immunoconjugates prepared under selected molar ratios were taken forward for characterization.

The impact of formulation composition and applied freeze-drying protocol on residual moisture was first evaluated. As shown in Table IV, the percentage of residual moisture varies with formulation composition, notably between the water- and saline-based F2-5 formulations. The water-based batch consistently showed higher moisture levels (5.10-6.06 %), while the saline-based batch exhibited lower moisture levels (1.90-5.01 %). This trend suggests that the presence of saline facilitates freezing and drying, thereby more efficiently removing residual water, as indicated by Matejtschuk *et al*. (29).

Uncorrected proofs

Formulation F1 showed residual moisture of ~5 % in both batches, which is in line with a buffer–mannitol system where 1 % mannitol predominantly acts as a crystalline bulking agent. To minimize the risk of pH shifts, formulation F2 consists of reduced buffer concentration (10 mmol $L^{-1}$) while retaining 1 % mannitol (30). Moisture remained unchanged in W.F2 but decreased to 2.73 % in S.F2, confirming that the presence of NaCl favors drying and results in lower residual moisture. To further protect the antibody integrity and reduce moisture, formulations F3-F5 were prepared without buffer salts (31). In these buffer-free formulations, sucrose was added at different ratios to modulate mannitol crystallization, and in F5, polysorbate 20 was added as a surfactant (32). These optimizations resulted in significantly lower moisture in S.F5, reaching a desirable level below 3 % (33).

Complete reconstitution was defined as the time required to obtain a clear solution, without visible particles, upon gentle swirling. Under these criteria, all formulations reconstituted rapidly (≤30 s) in saline, confirming the literature findings for low protein concentrations and formulations containing a crystalline bulking agent (34). The initial macroscopic appearance of the freeze-dried formulations resembles a compact cake, which readily collapses into a powder-like appearance after minimal agitation. This indicates limited cake robustness under the applied freeze-drying protocol and formulation composition, despite achieving the desired dryness. Nevertheless, the integrity of the formulations was confirmed by subsequent analytical characterization, indicating that the observed collapse did not adversely affect product quality.

As a preliminary experiment, radiolabeling with $^{177}$Lu was performed on all freeze-dried, water- and saline-based daratumumab immunoconjugates. Among the tested conjugates, the 30-fold daratumumab–*p*-SCN-Bn-DOTA showed the highest radiolabeling yield (99.8 %), with no observable difference between the batches. Based on these results, the subsequent evaluation of formulation-related effects on the antibody purity was limited to the 30-fold daratumumab–*p*-SCN-Bn-DOTA conjugate and assessed by SE-HPLC.

SE-HPLC results of the reconstituted formulations showed batch-dependent differences in purity between water- and saline-based preparations. Quantification was based on peak-area normalization, and the results were expressed as relative percentages of the main peak, low-molecular-mass species (LMWS, fragments), and high-molecular-mass species (HMWS, aggregates). The purity results are summarized in Table V, and corresponding overlay chromatograms are presented in Fig. 2. Taken together, HMWS formation was identified as the primary selection criterion, whereas LMWS levels remained consistently low and stable, and

Uncorrected proofs

monomer content remained above 95 % (35). Aggregates were detected in the first two formulations in both batches, with HMWS levels ranging from 4.80–5.90 % for F1 and 6.67–8.55 % for F2. In contrast, formulations F3 and F5 exhibited the highest purity profile, with monomer contents above 98.00 % in both batches, non-detectable HMWS, and minimal LMWS. The immunoconjugate in F4 remained predominantly as a monomer in water, with no detectable HMWS, but showed a slight HMWS formation in saline. These purity profiles highlight F3 and F5 as the most promising candidates for subsequent experiments and for optimizing radiolabeling efficiency.

Based on the results for formulation composition, residual moisture and purity, the saline-based formulation containing mannitol:sucrose (2:1) and polysorbate 20 (S.F5) was selected as the promising formulation for further evaluation.

As mentioned above, based on CAR, five candidates: 50-fold daratumumab–DOTA–NHS, 20- and 30-fold daratumumab–*p*-SCN-Bn-DOTA, and 20- and 30-fold daratumumab–*p*-SCN-Bn-1B4M-DTPA, were examined. For radiolabeling optimization, 0.1 mol $L^{-1}$ sodium acetate (pH 4.5) was selected as the reaction solvent for subsequent radiolabeling experiments based on overall performance. The results from the 50-fold daratumumab–DOTA–NHS showed a low radiolabeling yield (<30 %). The 20-fold [$^{177}$Lu]Lu-daratumumab-*p*-SCN-Bn-DOTA yielded 86.0 %, whereas the 30-fold reached 99.8 %. The radiolabeling yield for both daratumumab-*p*-SCN-Bn-1B4M-DTPA immunoconjugates exceeded 98.0 %, and the lower chelator excess was preferred to minimize chemical modification of the antibody, while also reducing excess reagent use and associated chemical waste, in line with green chemistry considerations (Fig. 3).

The radiolabeling yield for both compounds, 30-fold [$^{177}$Lu]Lu-daratumumab-*p*-SCN-Bn-DOTA and 20-fold [$^{177}$Lu]Lu-daratumumab-*p*-SCN-Bn-1B4M-DTPA, exceeded 98.0 %. Because of the high radiochemical purity and minimal presence of free $^{177}Lu^{3+}$, no additional purification was required, and both were used in subsequent *in vitro* stability evaluation.

The *in vitro* stability of the two radioimmunoconjugates, [$^{177}$Lu]Lu-daratumumab-*p*-SCN-Bn-DOTA and [$^{177}$Lu]Lu-daratumumab-*p*-SCN-Bn-1B4M-DTPA, was assessed by measuring the percentage of radioactivity bound to the antibody relative to the initial value at the start of the incubation. More than 95.93 % of the $^{177}$Lu remained attached to daratumumab-DOTA-SCN within 168 hours. In contrast, [$^{177}$Lu]Lu-daratumumab-*p*-SCN-Bn-1B4M-DTPA

Uncorrected proofs

showed significantly lower stability, with a notable decrease already after 48 hours, and only 51.91 % of the activity remaining bound to the antibody after one physical half-life of $^{177}$Lu.

The labeling efficiency was evaluated by incubation of the daratumumab–*p*-SCN-Bn-DOTA conjugate with $^{177}LuCl_3$ for a period of 5–60 min at 37 °C with gentle shaking. The developed iTLC chromatograms showed clear separation between the radiolabeled immunoconjugate retained at the origin ($R_f$ = 0) and [$^{177}$Lu]Lu-*p*-SCN-Bn-DOTA migrating toward the solvent front ($R_f$ = 1), and free [$^{177}$Lu]$Lu^{3+}$ ($R_f$ = 0.3-0.5).

Time-dependent incubation experiments showed an increase in labeling efficiency over time, reaching a plateau at 50–60 min, indicating effective coordination of the metal under the applied conditions (Fig. 4).

To verify that the antibody structure remains intact after conjugation and freeze-drying, ATR-FTIR spectra were evaluated, focusing on the Amide I (1700–1600 $cm^{-1}$) and Amide II (1580–1510 $cm^{-1}$) regions. Since excipient composition and residual moisture can significantly affect the mid-IR region, particularly where the water bending vibration overlaps with the Amide I band, placebo spectra were acquired as a control and used for spectral subtraction to improve interpretation of the protein bands. To further enhance band resolution, the second Savitzky–Golay derivative spectra were processed (36). The analysis of the Amide I band showed that the spectra of the purified freeze-dried daratumumab and the daratumumab-*p*-SCN-Bn-DOTA immunoconjugate were almost identical between 1700 and 1600 $cm^{-1}$ (Figs. S2, S3). In the second derivative spectra (Fig. 5), the dominant component remained centered around 1640 $cm^{-1}$ and no new assignments were identified, suggesting that the β-sheet-rich secondary structure of the IgG was preserved after both conjugation and freeze-drying. Importantly, no additional components in the 1610–1620 $cm^{-1}$ region, commonly associated with aggregation-related intermolecular β-sheet formation, were observed.

Raman spectra were evaluated in the Amide I (1600–1700 $cm^{-1}$) and Amide III (1200–1350 $cm^{-1}$) regions to confirm the structural integrity. Importantly, neither relevant peak shifts nor new bands were observed in the spectra of the purified, freeze-dried daratumumab and the daratumumab-*p*-SCN-Bn-DOTA immunoconjugate, which are sensitive to changes in secondary structure (Fig. 6).

Overall, the findings from both ATR-FTIR and Raman spectroscopy indicate that conjugation of DOTA-SCN and freeze-drying did not result in detectable structural changes or antibody aggregation.

Uncorrected proofs

To further confirm antibody integrity and distinguish fragmentation from aggregation, SDS-PAGE was performed under both reducing and non-reducing conditions. Protein bands were evaluated to assess the integrity of the intact antibody (~150 kDa) and its heavy (~50 kDa) and light (~25 kDa) chains. Under reducing conditions, all samples showed the expected heavy- and light-chain bands, with no additional LMWS. Under non-reducing conditions, a dominant band at ~150 kDa corresponding to intact IgG was observed, with no evident high-molecular-weight bands. Finally, the electrophoretic profiles support preserved structural integrity of the immunoconjugates, consistent with the SE-HPLC and vibrational spectroscopic findings (Fig. S4).

## CONCLUSIONS

Conjugation conditions for daratumumab were optimized in carbonate buffer for both BFCs: *p*-SCN-Bn-DOTA and *p*-SCN-Bn-1B4M-DTPA. Daratumumab-*p*-SCN-Bn-DOTA was selected for further physicochemical characterization based on its $^{177}$Lu radiolabeling yield and improved *in vitro* stability compared with the *p*-SCN-Bn-1B4M-DTPA analogue. The quality assessment of freeze-drying formulations showed that excipient and solvent selection strongly influence product characteristics. A saline-based, buffer-free sucrose–mannitol formulation containing polysorbate 20 (S.F5) showed the most favorable characteristics with low residual moisture, rapid reconstitution, and non-detectable HMW species.

From a pharmaceutical perspective, these findings support the development of a ready-to-use radiopharmaceutical kit and provide the basis for extending the approach to other diagnostic and therapeutic radionuclides. In addition, the developed formulation contributes to the translational advancement of theranostic strategies. Future work will focus on long-term stability evaluation, supported by predictive modeling approaches, and *in vivo* validation.

*Acronyms.* – ADCC – antibody-dependent cellular cytotoxicity, ADCP – antibody-dependent cellular phagocytosis, BFC – bifunctional chelator, CAR – chelator-to-antibody ratio, CDC – complement-dependent cytotoxicity, FTIR – Fourier transform infrared spectroscopy, HMWS – high molecular weight species, iTLC – instant thin-layer chromatography, LMWS – low molecular weight species, mAb – monoclonal antibody, PBS – phosphate-buffered saline, RCP – radiochemical purity, RIC – radioimmunoconjugate, SDS-PAGE – sodium dodecyl sulfate–polyacrylamide gel electrophoresis, SE-HPLC – size exclusion high-performance liquid chromatography

Uncorrected proofs

*Authors contributions.* – Conceptualization: PA, MAL, EJI; methodology: PA, SVĐ; EJI; investigation: PA, MAL, KD, MA, DK, PM, ISS; writing – original draft: PA, MAL; writing - review and editing: PA, MAL, KD, MA, DK, PM, IM, AD, SVĐ, EJI; project administration: EJI; supervision: SVĐ and EJI. All authors have read and agreed to the published version of the manuscript.

*Funding.* – This work was supported by the International Atomic Energy Agency (IAEA) CRP F22077 and by the Science Fund of the Republic of Serbia (Grant No. 7282, RADIOMAG).

*Conflict of interest.* – The authors declare no conflict of interest.

*Acknowledgements*. – The authors acknowledge the institutional support and access to facilities provided by the Faculty of Medical Sciences, Goce Delcev University, Stip, North Macedonia.

Supplementary materials are available upon request.

REFERENCES

1. A. Vaillant, B. R. Pandit, C. Unakal, S. Vuma and P. E. Akpaka, A comprehensive review about the use of monoclonal antibodies in cancer therapy, *Antibodies* **14**(2) (2025) Article ID 35 (25 pages); https://doi.org/10.3390/antib14020035

2. K. Toledo-Stuardo, C. H. Ribeiro, F. González-Herrera, D. J. Matthies, M. S. Le Roy, C. Dietz-Vargas, Y. Latorre, I. Campos, Y. Guerra, S. Tello, V. Vásquez-Sáez, P. Novoa, N. Fehring, M. González, J. Rodríguez-Siza, G. Vásquez, P. Méndez, C. Altamirano and M. C. Molina, Therapeutic antibodies in oncology: an immunopharmacological overview, *Cancer Immunol. Immunother*. **73** (2024) Article ID 242 (22 pages); https://doi.org/10.1007/s00262-024-03814-2

3. European Medicines Agency, *EU/3/03/136 – Orphan designation: iodine ($^{131}I$) tositumomab for the treatment of follicular lymphoma*, EMA, Amsterdam, May 2015; https://www.ema.europa.eu/en/medicines/human/orphan-designations/eu-3-03-136; last access date January 11, 2026

4. European Medicines Agency, *Zevalin: EPAR — Medicine overview*, EMA, Amsterdam, Sept 2011; https://www.ema.europa.eu/en/medicines/human/EPAR/zevalin; last access date January 11, 2026

5. S. V. Rajkumar, M. A. Dimopoulos, A. Palumbo, J. Blade, G. Merlini, M. V. Mateos, S. Kumar, J. Hillengass, E. Kastritis, P. Richardson, O. Landgren, B. Paiva, A. Dispenzieri, B. Weiss, X. Leleu, S. Zweegman, S. Lonial, L. Rosinol, E. Zamagni, S. V. Rajkumar, J. San Miguel and K. C. Anderson, International Myeloma Working Group updated criteria for the diagnosis of multiple myeloma, *Lancet Oncol*. **15** (2014) e538–e548; https://doi.org/10.1016/S1470-2045(14)70442-5

6. J. H. Yi, D. H. Yoon, S. Park, H. K. Kim, J. S. Kim, S. S. Yoon, K. Kim, C. K. Min, S. J. Lee, S. J. Lee, K. H. Lee, J. H. Lee, D. H. Yang, J. J. Lee, H. J. Kim and J. J. Lee, Real-world outcomes

Uncorrected proofs

of SLiM-only multiple myeloma: Korean multicenter retrospective analysis (KMM2401 study), *Ann. Hematol.* **105** (2026) Article ID 93 (8 pages); https://doi.org/10.1007/s00277-026-06851-2

7. K. Ghaffari, A. Moradi Hasan-Abad, M. Etedali, S. Alizadeh and A. Ghasemi, Hematologic malignancies and an overview of emerging therapies for hematologic malignancies: a systematic review, *Cancer Treat. Res. Commun.* **46** (2026) Article ID 101074 (16 pages); https://doi.org/10.1016/j.ctarc.2025.101074

8. M. C. Palanca-Wessels and O. W. Press, Advances in the treatment of hematologic malignancies using immunoconjugates, *Blood* **123**(15) (2014) 2293–2301; https://doi.org/10.1182/blood-2013-10-492223

9. European Medicines Agency, *Darzalex (daratumumab) — EPAR — Medicine overview*, EMA, Amsterdam, Aug 2025; https://www.ema.europa.eu/en/medicines/human/EPAR/darzalex; last access date December 1, 2025

10. U. S. Food and Drug Administration, *DARZALEX FASPRO™ (daratumumab and hyaluronidase-fihj) injection, for subcutaneous use – Prescribing information*, US FDA, Silver Spring (MD, USA), May 2020; https://www.accessdata.fda.gov/drugsatfda_docs/label/2020/761145s000lbl.pdf; last access date January 11, 2026

11. European Medicines Agency, *Sarclisa – EPAR – Medicine overview*, EMA, Amsterdam, Aug 2025; https://www.ema.europa.eu/en/medicines/human/EPAR/sarclisa; last access date January 11, 2026

12. M. de Weers, Y.-T. Tai, M. S. van der Veer, J. M. Bakker, T. Vink, D. C. Jacobs, L. A Oomen, M. Peipp, T. Valerius, J. W Slootstra, T. Mutis, W. K. Bleeker, K. C. Anderson, H. M. Lokhorst, J. G. J. van de Winkel, P. W. H. I. Parrenl, Daratumumab, a novel therapeutic human CD38 monoclonal antibody, induces killing of multiple myeloma and other hematological tumors, *J. Immunol.* **186** (2011) 1840–1848; https://doi.org/10.4049/jimmunol.1003032

13. S. Yadav, S. Gundeti, A. Bhave, U. Deb, J. Dixit and K. Mishra, Role of daratumumab in the frontline management of multiple myeloma: a narrative review, *Expert Rev. Hematol.* **16**(10) (2023) 743–760; https://doi.org/10.1080/17474086.2023.2246651

14. C. Wang, Z. Xu, M. Jiang, Y. Chen and Y. Lan, Efficacy and safety of isatuximab combination therapy in multiple myeloma: a meta-analysis of randomized controlled trials, *Cancers* **17**(21) (2025) Article ID 3494 (15 pages); https://doi.org/10.3390/cancers17213494

15. J. Jureczek, K. Kałwak and P. Dzięgiel, Antibody-based immunotherapies for the treatment of hematologic malignancies, *Cancers* **16**(24) (2024) Article ID 4181 (24 pages); https://doi.org/10.3390/cancers16244181

Uncorrected proofs

16. S. V. Rajkumar, M. A. Dimopoulos, A. Palumbo, J. Blade, G. Merlini, M. V. Mateos, S. Kumar, J. Hillengass, E. Kastritis, P. Richardson, F. Landgren, B. Durie, R. A. Kyle, and International Myeloma Working Group, International Myeloma Working Group updated criteria for the diagnosis of multiple myeloma, *Blood* **131**(1) (2018) 13–20; https://doi.org/10.1182/blood-2017-06-740944

17. M. Minnix, V. Adhikarla, E. Caserta, E. Poku, R. Shively and F. Pichiorri, Comparison of CD38-targeted α- versus β-radionuclide therapy of disseminated multiple myeloma in an animal model, *J. Nucl. Med*. **62** (2021) 795–801; https://doi.org/10.2967/jnumed.120.251983

18. W. Dawicki, K. J. Allen, R. Jiao, M. E. Malo, M. Helal, M. S. Berger D. L. Ludwig and E. Dadachova, Daratumumab-$^{225}$Actinium conjugate demonstrates greatly enhanced antitumor activity against experimental multiple myeloma tumors, *Oncoimmunology* **8**(8) (2019) Article ID 1607673 (9 pages); https://doi.org/10.1080/2162402X.2019.1607673

19. I. Quelven, J. Monteil, M. Sage, A. Saidi, J. Mounier, A. Bayout, J.Garrier, M. Cogne and S. Durand-Panteixal, $^{212}$Pb α-radioimmunotherapy targeting CD38 in multiple myeloma: a preclinical study, J. *Nucl. Med.* **61**(7) (2020) 1058–1065; https://doi.org/10.2967/jnumed.119.239491

20. S. Li, C. G. England, E. B. Ehlerding, C. J. Kutyreff, J. W. Engle, D. Jiang and W. Cai, ImmunoPET imaging of CD38 expression in hepatocellular carcinoma using $^{64}$Cu-labeled daratumumab, *Am. J. Transl. Res*. **11**(9) (2019) 6007–6015.

21. E. Caserta, J. Chea, M. Minnix, E. K. Poku, D. Viola, S. Vonderfecht, P. Yazaki, D. Crow, J. Khalife, J. F. Sanchez, J. M. Palmer, S. Hui, N. Carlesso, J. Keats, Y. Kim, R. Buettner, G. Marcucci, S. Rosen, J. Shively, D. Colcher, A. Krishnan and F. Pichiorri, Copper-64–labeled daratumumab as a PET/CT imaging tracer for multiple myeloma, *Blood* **131**(7) (2018) 741-745; https://doi.org/10.1182/blood-2017-09-807263

22. A. F. Viana and E. Cannarozzo, Theranostics explained: a personalized approach to cancer care, *J. Nucl. Med.* **67**(4) (2026) 494–495; https://doi.org/10.2967/jnumed.125.271895

23. L. Kang, C. Li, Z. T. Rosenkrans, N. Huo, Z. Chen, E. B. Ehlerding, Y. Huo, C. A. Ferreira, T. E. Barnhart, J. W. Engle, R. Wang, D. Jiang, X. Xu and W. Cai, CD38-targeted theranostics of lymphoma with $^{89}$Zr/$^{177}$Lu-labeled daratumumab, *Adv. Sci.* **8** (2021) Article ID 2001879 (13 pages); https://doi.org/10.1002/advs.202001879

24. M. Sterjova, P. Džodić, P. Makreski, J. Živković and E. Janevik-Ivanovska, Electrophoresis and Raman spectroscopy characterization of integrity and secondary structure of p-SCN-Bn-DTPA- and p-SCN-Bn-1B4M-DTPA-conjugated trastuzumab, *Farmacia* **67**(4) (2019) 621–626; https://doi.org/10.31925/farmacia.2019.4.10

Uncorrected proofs

25. M. Sterjova, P. Džodić, P. Makreski, A. Duatti, M. Risteski and E. Janevik-Ivanovska, Vibrational spectroscopy as a tool for examination to the secondary structure of metal-labeled trastuzumab immunoconjugates, *J. Radioanal. Nucl. Chem.* **320** (2019) 209–218; https://doi.org/10.1007/s10967-019-06450-8

26. U. Karczmarczyk, A. Sawicka, P. Garnuszek, M. Maurin and W. Wojdowska, Does the number of bifunctional chelators conjugated to a mAb affect the biological activity of its radio-labeled counterpart? Discussion using the example of mAb against CD-20 labeled with $^{90}$Y or $^{177}$Lu, J. *Med. Chem.* **65**(9) (2022) 6419–6430; https://doi.org/10.1021/acs.jmedchem.1c02044

25. L. Kang, C. Li, Z. T. Rosenkrans, N. Huo, Z. Chen, E. B. Ehlerding, Y. Huo, C. A. Ferreira, T. E. Barnhart, J. W. Engle, R. Wang, D. Jiang, X. Xu and W. Cai, CD38-targeted theranostics of lymphoma with $^{89}$Zr/$^{177}$Lu-labeled daratumumab, *Adv. Sci.* **8** (2021) Article ID 2001879 (13 pages); https://doi.org/10.1002/advs.202001879

26. M. Sterjova, P. Džodić, P. Makreski, J. Živković and E. Janevik-Ivanovska, Electrophoresis and Raman spectroscopy characterization of integrity and secondary structure of p-SCN-Bn-DTPA- and p-SCN-Bn-1B4M-DTPA-conjugated trastuzumab, *Farmacia* **67**(4) (2019) 621–626; https://doi.org/10.31925/farmacia.2019.4.10

27. G. Giannini, F. M. Milazzo, G. Battistuzzi, M. Lanza, D. Pirolli, S. Carradori and R. De Santis, Synthesis and preliminary in vitro evaluation of DOTA-Tenatumomab conjugates for theranostic applications in tenascin expressing tumours, *Bioorg. Med. Chem.* **27**(15) (2019) 3248–3253; https://doi.org/10.1016/j.bmc.2019.05.047

28. J. A. Delage, A. Faivre-Chauvet, J. Barbet, J. K. Fierle, N. Schaefer, G. Coukos, D. Viertl, S. M. Dunn, S. Gnesin and J. O. Prior, Impact of DOTA conjugation on pharmacokinetics and immunoreactivity of [$^{177}$Lu]Lu-1C1m-Fc, an anti TEM-1 fusion protein antibody in a TEM-1 positive tumor mouse model, *Pharmaceutics* **13**(1) (2021) Article ID 96 (19 pages); https://doi.org/10.3390/pharmaceutics13010096

29. P. Matejtschuk, C. Bird, E. Ezeajughi, K. MacLellan-Gibson and M. Wadhwa, Impact of formulation choices on the freeze-drying of an interleukin-6 reference material, *Front. Mol. Biosci.* **9** (2022) Article ID 868460 (9 pages); https://doi.org/10.3389/fmolb.2022.868460

30. Y. Cheng, H. T. Duong, Q. Hu, M. Shameem and X. C. Tang, Practical advice in the development of a lyophilized protein drug product, *Antibody Ther.* **8**(1) (2025) 13–25; https://doi.org/10.1093/abt/tbae030

31. T. T. Mutukuri, J. Ling, Y. Du, Y. Su and Q. T. Zhou, Effect of buffer salts on physical stability of lyophilized and spray-dried protein formulations containing bovine serum albumin and trehalose, *Pharm. Res.* **40**(6) (2023) 1355–1371; https://doi.org/10.1007/s11095-022-03318-7

Uncorrected proofs

513 32. M. Bjelošević and P. Ahlin Grabnar, Effects of monoclonal-antibody concentration and type of
514 bulking agent on critical quality attributes of lyophilisates, *J. Drug Deliv. Sci. Technol*. **63** (2021)
515 Article ID 102510; https://doi.org/10.1016/j.jddst.2021.102510

516 33. United States Pharmacopeia, *USP <922> Water Activity: A Better Approach for Lyo Moisture*
517 *Determination – Applications enabled by rapid non-destructive headspace moisture analysis of*
518 *freeze-dried product*, USP, Rockville (MD, USA), March 30, 2018;
519 https://www.uspnf.com/notices/922-water-activity; last access date January 10, 2026

520 34. J. Horn, J. Schanda and W. Friess, Impact of fast and conservative freeze-drying on product quality
521 of protein–mannitol–sucrose–glycerol lyophilizates, *Eur. J. Pharm. Biopharm*. **127** (2018) 342–
522 354; https://doi.org/10.1016/j.ejpb.2018.03.003

523 35. L. Knoll, J. Thiesen, M. D. Klassen, L. M. Reinders, J. Türck and I. Kraemer, In-use stability of
524 ready-to-administer daratumumab subcutaneous injection solution in plastic syringes, *Eur. J. Hosp.*
525 *Pharm.* **32** (2025) 154–161; https://doi.org/10.1136/ejhpharm-2023-003883

526 36. H. Godzo, O. Gigopulu, J. Acevska, N. Geskovski, A. P. Panovska, B. Acevski, F. Dimoska, M.
527 Nuneva and K. Brezovska, Application of ATR-FTIR as a screening method for analysis of
528 biopharmaceutical preparations containing trastuzumab, *Maced. Pharm. Bull*. **69** (Suppl. S1)
529 (2023) 253–254; https://doi.org/10.33320/maced.pharm.bull.2023.69.03.124
530

Uncorrected proofs

531

532

533

Uncorrected proofs

534

535

Uncorrected proofs

*Table I. Composition of freeze-drying formulations*

| | |
|---|---|
| Formulation 1 | 0.1 mol $L^{-1}$ PBS, pH=8.0; 1 % (*m*/*V*) mannitol |
| Formulation 2 | 0.01 mol $L^{-1}$ PBS, pH=8.0; 1 % (*m*/*V*) mannitol |
| Formulation 3 | Sucrose:mAb = 1:450; mannitol:sucrose = 2:1 |
| Formulation 4 | Sucrose:mAb = 1:450; mannitol:sucrose = 4:1 |
| Formulation 5 | Sucrose:mAb = 1:450; mannitol:sucrose = 2:1; 0.02 % (*V*/*V*) polysorbate 20 |

Batch W: ultra-pure water as solvent
Batch S: 0.9 % NaCl as solvent

Uncorrected proofs

541
542

*Table II. Freeze-drying protocol parameters (temperature, ramp rate, and hold time) for each segment*

| | |
|---|---|
| SEGMENT 1 | Freezing: -40 °C |
| | Ramping 1 °C $min^{-1}$ |
| | Hold 3 h |
| SEGMENT 2 | Annealing: -10 °C |
| | Ramping 0.5 °C $min^{-1}$ |
| | Hold 2 h |
| SEGMENT 3 | Freezing: -40 °C |
| | Ramping 1 °C $min^{-1}$ |
| | Hold 1.5 h |
| SEGMENT 4 | Primary drying: -10 °C |
| | Ramping 0.15 °C $min^{-1}$ |
| | Hold 18 h |
| SEGMENT 5 | Secondary drying: +25 °C |
| | Ramping 0.15 °C $min^{-1}$ |
| | Hold 8 h |
| Total ca 50 hours | |

543
544

Uncorrected proofs

*Table III. Average CAR values of daratumumab immunoconjugates*

| Immunoconjugate | Conjugation in phosphate buffer (pH 8.5) | Conjugation in carbonate buffer (pH 8.5) |
|---|---|---|
| Daratumumab-DOTA-NHS 1:20 | 0.00 | 0.18 |
| Daratumumab-DOTA-NHS 1:30 | 0.00 | 0.10 |
| Daratumumab-DOTA-NHS 1:50 | 0.20 | 0.46 |
| Daratumumab-DOTA-SCN 1:20 | 1.27 | 2.31 |
| Daratumumab-DOTA-SCN 1:30 | 1.75 | 2.66 |
| Daratumumab-DOTA-SCN 1:50 | 2.76 | 3.77 |
| Daratumumab-1B4M DTPA 1:20 | 0.40 | 0.36 |
| Daratumumab-1B4M DTPA 1:30 | 0.65 | 0.76 |
| Daratumumab-1B4M DTPA 1:50 | 0.78 | 0.85 |

*Table IV. Residual moisture in freeze-dried formulations*

| | Residual moisture (%) | |
|---|---|---|
| Formulation | Batch W | Batch S |
| F1 | 5.54 | 5.01 |
| F2 | 5.60 | 2.73 |
| F3 | 6.06 | 2.17 |
| F4 | 6.05 | 2.83 |
| F5 | 5.10 | 1.90 |

Uncorrected proofs

*Table V. Purity profile of water-based (W) and saline-based (S) batches*

| Formulation | Main monomer (%) | | High molecular mass species (%) | | Low molecular mass species (%) | |
|---|---|---|---|---|---|---|
| | W | S | W | S | W | S |
| 1 | 93.86 | 94.98 | 5.90 | 4.80 | 0.24 | 0.22 |
| 2 | 93.01 | 91.23 | 6.67 | 8.55 | 0.23 | 0.22 |
| 3 | 99.76 | 99.75 | n.d.* | n.d. | 0.24 | 0.25 |
| 4 | 99.73 | 98.90 | n.d. | 0.85 | 0.27 | 0.25 |
| 5 | 99.76 | 99.75 | n.d. | n.d. | 0.24 | 0.25 |

*n.d. – non-detectable (no peak observed in the predefined HMWS retention-time region under the applied SE-HPLC conditions)

Uncorrected proofs

555

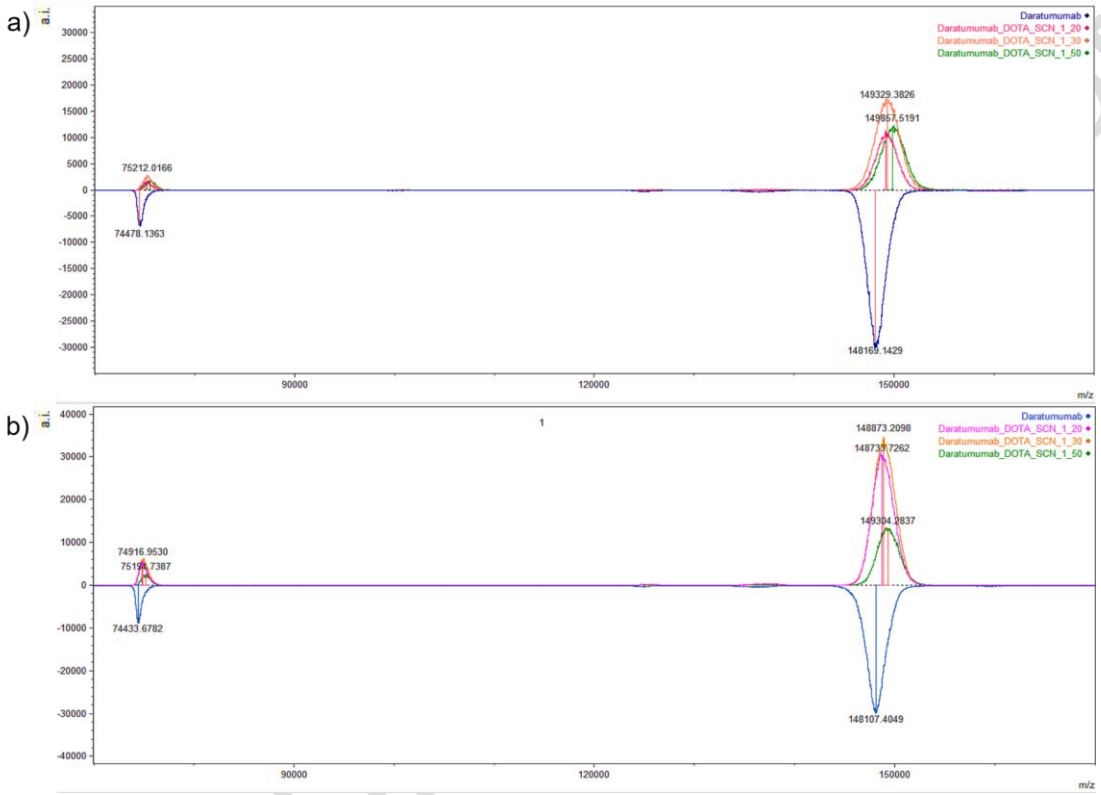


556

557 Fig. 1. MALDI-TOF MS of daratumumab-*p*-SCN-Bn-DOTA conjugates in: a) phosphate buffer and b) carbonate buffer. Numbers shown refer to the center of

558 the peaks. Peaks with ~75 kDa are the doubly charged molecular ions displaying the half-MWs daratumumab-*p*-SCN-Bn-DOTA conjugates.

**Commented [Ma1]:** Ordinate markation

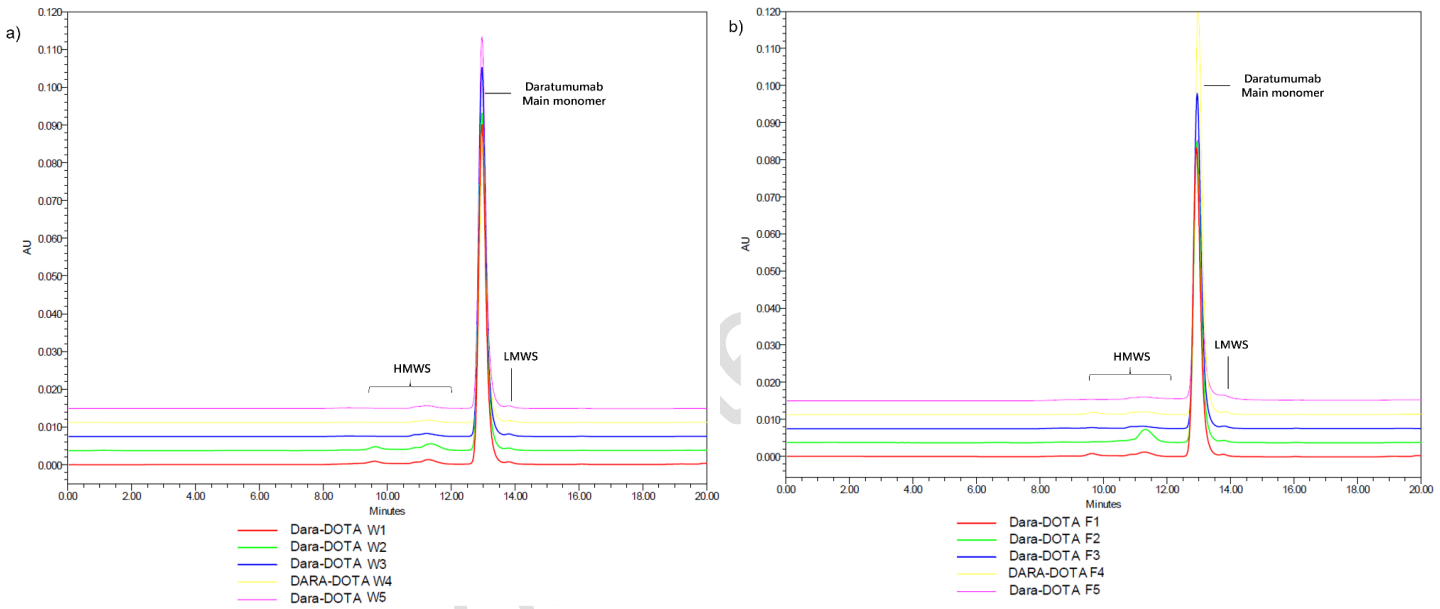


Fig. 2. Overlay SE-HPLC chromatograms: a) W.F1-5 and b) S.F1-5 batches. The main monomer peak at $t_R \approx 13$ min, HMWS at $t_R \approx 9$ and 11 min, and LMWS at $t_R \approx 14$ min.

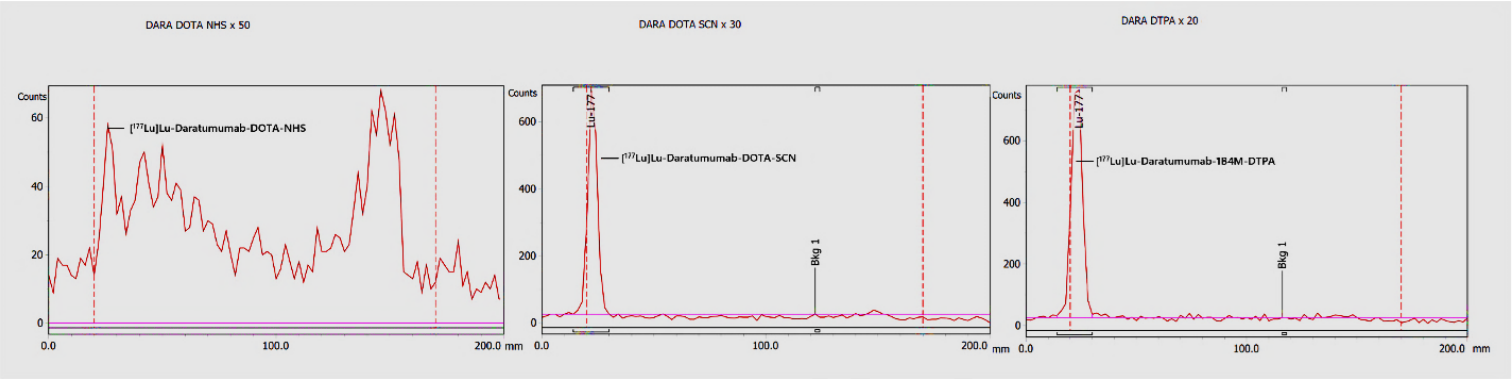


Fig. 3. Representative radiochromatograms of: a) 50-fold [$^{177}$Lu]Lu-daratumumab-DOTA-NHS, b) 30-fold [$^{177}$Lu]Lu-daratumumab-*p*-SCN-Bn-DOTA and c) 20-fold [$^{177}$Lu]Lu-daratumumab-*p*-SCN-Bn-1B4M-DTPA.

Uncorrected

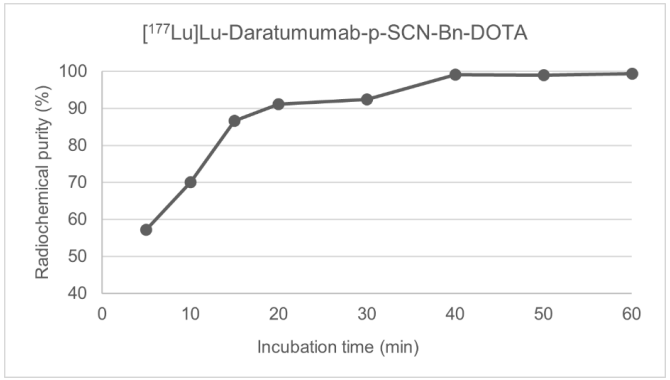


Fig. 4. $^{177}$Lu-labelling efficiency of daratumumab-*p*-SCN-Bn-DOTA (representative measurements).

**Commented [PA2]:** This figure is moved to the Supplementary file.

**Commented [PA3]:** This figure is moved to the Supplementary file.

Uncorrected proofs

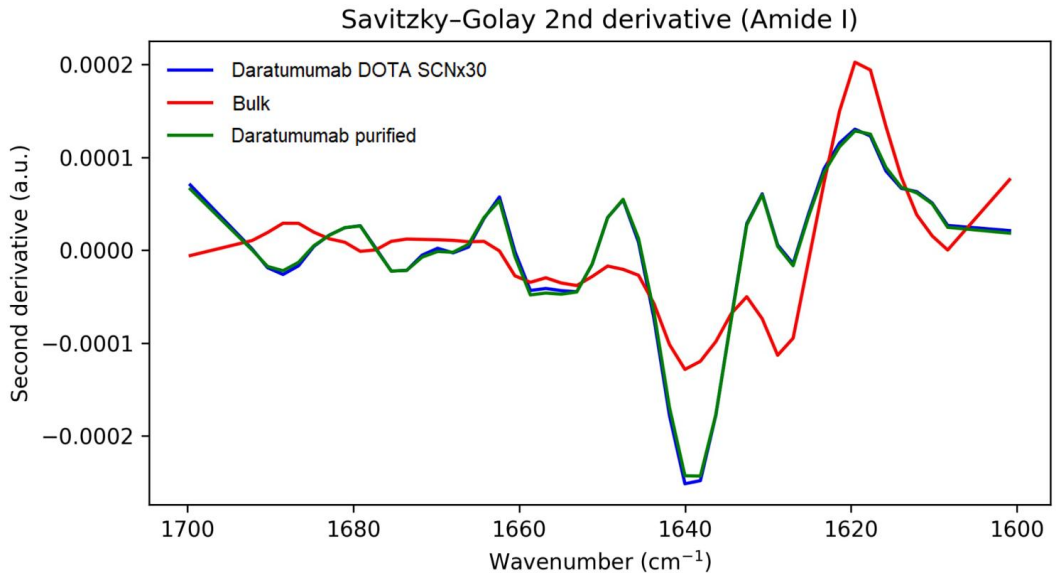


575

576 Fig. 5. Second derivative spectra.

577

Uncorrected Proofs

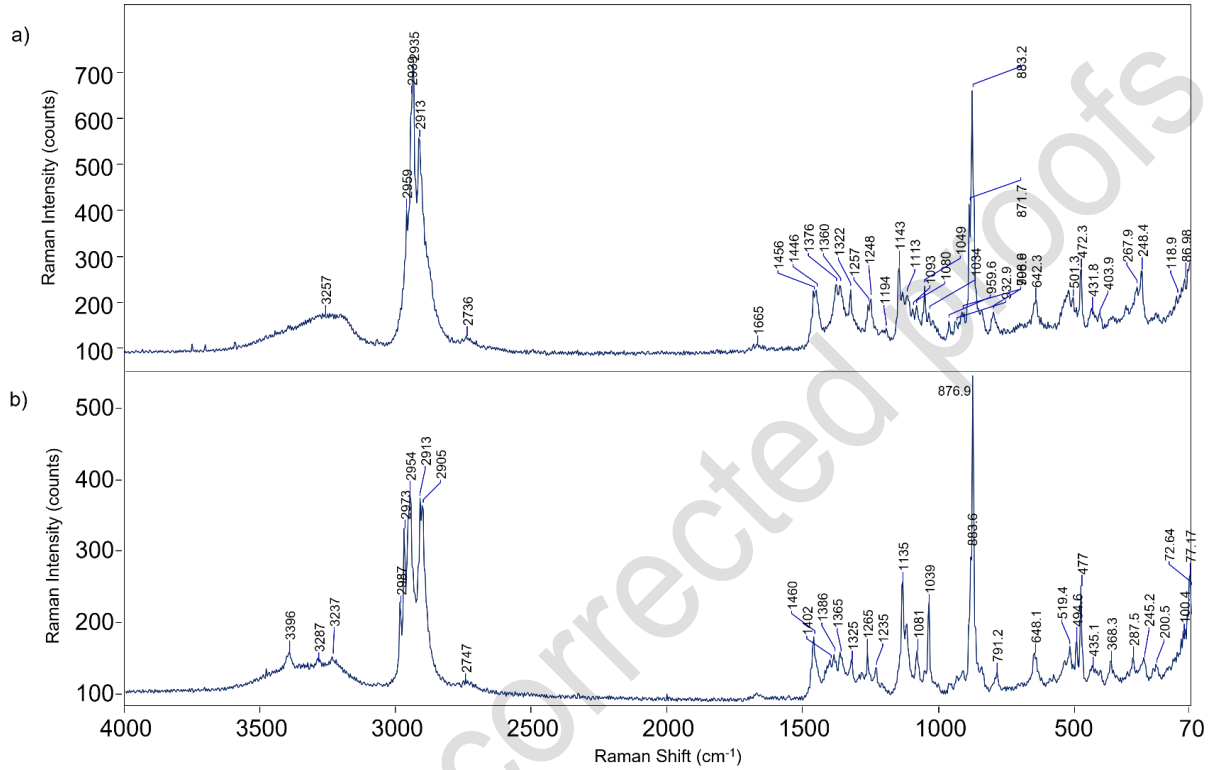


Fig. 6. Representative Raman spectra of: a) purified daratumumab and b) daratumumab-*p*-SCN-Bn-DOTA immunoconjugate.

Uncorrected Proofs